Jia *et al. Chin. J. Mech. Eng.* (2019) 32:6
https://doi.org/10.1186/s10033-019-0316-z

Chinese Journal of Mechanical Engineering

ORIGINAL ARTICLE

Open Access

Numerical Simulation and Experimental Research on Microstructural Evolution During Compact Hot Extrusion of Heavy Caliber Thick-Wall Pipe

Lu Jia[1,2], Yongtang Li[2,3*], Tianjing Hui[2,3] and Yang Zhang[4]

Abstract

Compact hot extrusion (CHE) process of heavy caliber thick-wall pipe is a new material-saving production process. In order to reveal the optimum hot extrusion parameters in CHE process, the effects of the extrusion parameters on the microstructural evolution are investigated systematically. The metadynamic recrystallization (MDRX) kinetic models and grain size models of as-cast P91 steel are established for the first time according to the hot compression tests performed on the Gleeble-3500 thermal-simulation machine. Then a thermal-mechanical and micro-macro coupled hot extrusion finite element (FE) model is established and further developed in DEFORM software. The results indicated that the grain size of the extruded pipe increases with the increasing of initial temperature and extrusion speed, decreases when extrusion ratio increases. Moreover, the grain size is more sensitive to the initial temperature and the extrusion ratio. The optimum hot extrusion parameters are including that, the initial extrusion temperature of 1250 °C, the extrusion ratio of 9 and the extrusion speed of 50 mm/s. Furthermore, in order to verify the simulation precisions, hot extrusion experiment verification on the heavy caliber thick-wall pipe is carried out on the 500 MN vertical hot extrusion equipment. The load–displacement curve of the extrusion process and the grain sizes of the middle part extruded pipe are in good accuracy with the simulation results, which confirms that the hot extrusion FE models of as-cast P91 steel could estimate the hot extrusion behaviors. The proposed hot extrusion FE model can be used to guide the industrial production research of CHE process.

Keywords: Heavy caliber thick-wall pipe, Compact hot extrusion process, Microstructural evolution, Numerical simulation, Average grain size

1 Introduction

Heavy caliber thick-wall pipes are the critical and basic components of large supercritical thermal power generator, nuclear power and petrochemical engineering. The current production technology on heavy caliber thick-wall pipe is mainly the punching and hot extrusion (PHE) process shown in Figure 1 [1–3]. This PHE process has several defects such as long production cycle, serious waste in material and investments of large scale equipment. In order to solve these disadvantages, Refs. [4, 5] propose a new compact hot extrusion (CHE) process shown in Figure 2. Compared with the PHE process, the CHE process could save up to 30% materials, and shorten at least half of the production period. It also presents advantages of energy conservation and pollution emission reduction.

Hot extrusion process is a complicated large deformation process which coupled with thermo-mechanical and microstructure evolutions. The as-cast billet is under the severe three-dimensional stress state, which contributes to the homogeneous plastic deformation and the fully exploited metal performance. The pipe could not only meet the industrial requirements in shape and

*Correspondence: liyongtang@tyust.edu.cn
[2] Shanxi Key Laboratory of Metallic Materials Forming Theory and Technology, Taiyuan University of Science and Technology, Taiyuan 030024, China
Full list of author information is available at the end of the article

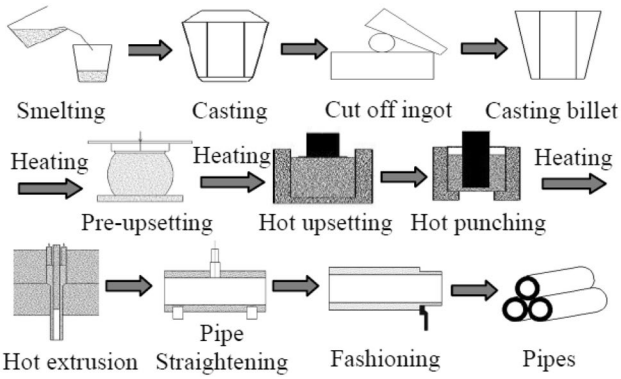

Figure 1 Punching and hot extrusion process

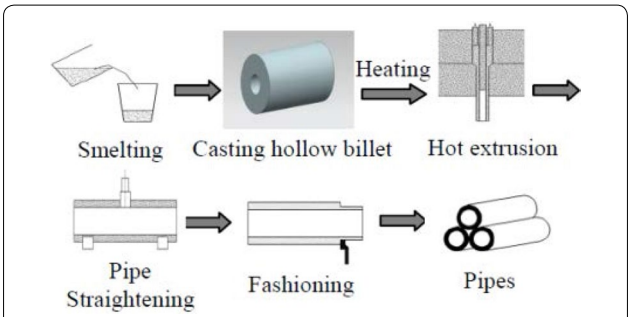

Figure 2 Compact hot extrusion process

size, but also is improved in mechanical properties and internal structures. The microstructural changes affect the mechanical characteristics of the materials. Thus, to obtain the thick-wall pipe with high performance and excellent mechanical properties in short production process, the microstructural evolution mechanism of as-cast billet during hot extrusion is required to be further investigated.

Compared with the experiments research, the numerical simulation is the efficient and economical alternative method for studying the engineering problems. Many researchers [6–8] have studied the technological parameters, microstructure evolution and mechanical properties of heavy caliber thick-wall pipe during hot extrusion. Dang et al. [9] developed the thermal-mechanical and dynamic recrystallization (DRX) coupled finite element (FE) model for the hot extrusion process of Inconel 625 pipe, and revealed the influence rules of the key parameters on the average DRX grain size. Chang et al. [10] used the FE method to simulate the process of asymmetric hot extrusion, the strain rate during the extrusion was proposed as a key parameter to the grain size. Jiang et al. [11] developed the phenomenological model for the effect of strain rate on recrystallization and grain growth kinetics in the 617B alloy, and the simulated microstructure agrees well with the actual manufactured pipe. Sathishkumar et al. [12] studied the extrusion ratio at different billet temperature on the plastic strain and strain rate of aluminium matrix composite during hot extrusion by FE analysis. Tang et al. [13] established the Arbitrary Lagrangian–Eulerian (ALE) method to investigate the influence of extrusion process on texture development of alloys. The study proposed that the method can be used as a useful tool in optimizing the extrusion process. In these categories of study, the dominant attention has been paid to the hot extrusion behaviors on the as-forged billet, which cannot be applied to the research of hot extrusion in CHE process. This is due to the fact that, the performance and mechanical properties of the as-forged billet have been improved before hot extrusion, and the main function of the extrusion process is the shape controlling. While the extruded work piece in CHE process is the as-cast billet, which demoulding under high temperature and directly squeezed under the extrusion temperature. The main purpose of CHE process is to realize the integration on shape forming and performance improving during the extrusion. Therefore, the investigations on the effects of the hot extrusion parameters on the deformation behaviors and microstructural evolution of as-cast alloy are significant to the workability and application on the CHE process.

For numerical simulations, it is necessary to establish the deformation constitutive models and microstructural evolution models of the materials firstly. P91 martensite heat-resistant steel is one of the leading materials in manufacturing industry of heavy caliber thick-wall pipe [14–17], and as-cast P91 alloy was employed as the raw materials in this study. Jia et al. [18] proposed that DRX was the main softening mechanism during hot extrusion. While Lin et al. [19–23] indicated that the static recrystallization (SRX) and metadynamic recrystallization (MDRX) will exist after hot deformation. When the strain reaches to the critical strain, the softening process after deformation is MDRX, in contrary the value of the strain is lower than the critical strain the SRX occurs. Although the extrusion process is completed with the materials flow out of the extrusion container, but the microstructures of the extruded pipe are still changing. In Ref. [24], the DRX evolution behaviors of as-cast P91 alloy was studied and the DRX simulation analysis during the hot extrusion indicated that the strains during extrusion process are all above the critical strain. Thus, the main softening mechanism after hot extrusion is MDRX. Moreover, the pipes will have grain growth under high temperature as well. Thus, the microstructural evolutions of the hot extrusion process are much more complicated. The microstructural evolution models of as-cast P91 alloy

Table 1 Chemical composition of P91 alloy (wt.%)

Element	C	Si	Mn	P	S	Cr
Content	0.084	0.28	0.38	0.019	0.005	8.63
Element	Ni	Mo	V	Nb	Al	N
Content	0.21	0.96	0.21	0.084	0.009	0.031

Table 2 Deformation parameters in compression test

Deformation parameters	Temperature T (°C)	Strain rate $\dot{\varepsilon}$ (s^{-1})	Strain ε (%)	Inter-pass time T (s)
	1100, 1150, 1200	0.01, 0.05, 0.1	0.3, 0.4, 0.5	2, 5, 30

steel during hot extrusion are still incomplete based on the researcher of Refs. [25, 26]. Moreover, it is necessary to reveal the influence regularity of extrusion parameters on the microstructural evolution during hot extrusion for controlling the microstructures of the extruded pipes.

In this study, the MDRX kinetic equations and grain size model of as-cast P91 alloy steel are established for the first time. The coupled hot extrusion FE model combined with thermal-mechanical and microstructural evolution models are developed and encoded in DEFORM software for the hot extrusion simulation. Based on the FE simulation results, the effects of the extrusion parameters impacting upon the grain sizes are revealed and the optimum extrusion parameters are proposed. In order to verify the simulation precisions, the hot extrusion experiment of as-cast billet is carried out and the comparisons between the simulated and the experimental results are presented. Finally, a brief conclusion is given in Section 6.

2 Hot Compression Experimental Procedure

The chemical composition of as-cast P91 alloy steel is shown in Table 1. The standard cylindrical specimens were machined with 8 mm in diameter and 12 mm in height. The two-pass isothermal hot compression tests were conducted on the Gleeble-3500 thermal-simulation machine, the experimental procedures can be found in Figure 3.

The specimens were heated to 1200 °C at the heating rate of 5 °C/s, and held for 5 min to ensure the fully austenitizing and elements were completely dissolved into solid solution. Then it cooled at the cooling rate of 5 °C/s to the deformation temperature and held for 1 min. In the following, the first stage compressions were applied in different deformation conditions (illustrated in Table 2). After deformation, the specimens were held under the deformation temperature for different inter-pass time t (2 s, 5 s and 30 s). Finally, the specimens were re-compressed under the same deformation conditions with the first stage. After the second compression, the deformed specimens were rapidly quenched in water.

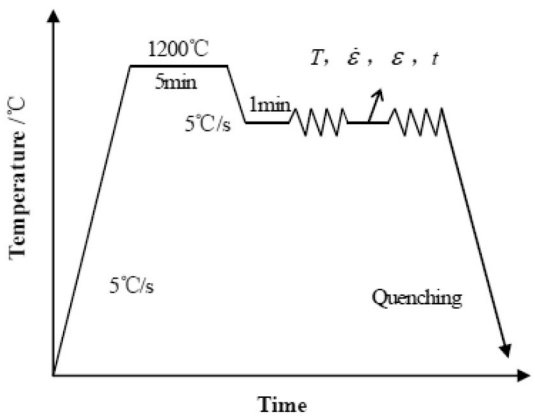

Figure 3 Experimental procedures of two-pass isothermal hot compression tests

The specimens were sectioned parallel to the compression axis. The sections were polished and electrolytic corrosion in the mixed-liquid of nitric acid (8 mL), hydrochloric acid (12 mL) and ethanol (100 mL). The metallographic microstructures in the section plane were taken and the average grain sizes were measured by linear intercept method.

3 Hot Compression Results and Analysis

3.1 MDRX Behaviors of As-cast P91 Alloy

The true stress-strain curves of two-pass isothermal hot compression tests are given in Figure 4. The deformation degrees in these tests were 26%, 33% and 40% (the strains are 0.3, 0.4 and 0.5 respectively, and the strains are both larger than the critical strain [26]), which indicate that the main softening mechanism in the unloading periods are MDRX. It can be obtained in Figure 4, the flow stresses of second deformation stages are smaller than the first stages. This is due to that, the MDRX softening during the inter-pass period has counteracted the residual work hardening of the first deformation, so in the second deformation stage, there needs fewer work hardenings to balance the DRX softening.

From Figure 4(a), the flow stresses of second deformation stages generally decrease as the inter-pass time increase under the same deformation conditions. What's more, the deformation temperature and strain rate have pronounced effects on the flow stress of as-cast P91 alloy steel. As illustrated in Figure 4(b), the flow stresses have a dramatic decrease with the increase of temperature. Besides, the deformation resistance of P91 alloy steel is sensitive to the temperature. Under low deformation temperature, the work hardening and the deformation

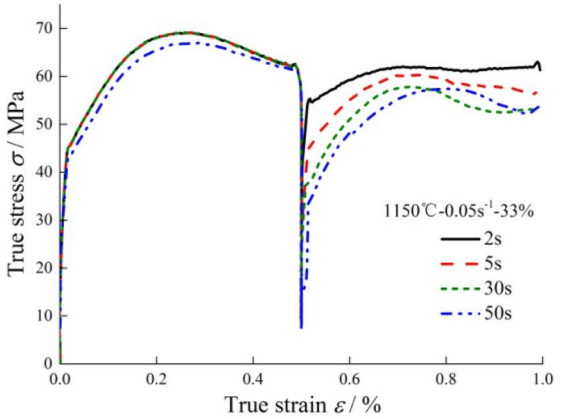

a Different inter-pass times under 1150 °C-0.05 s^{-1}-33%

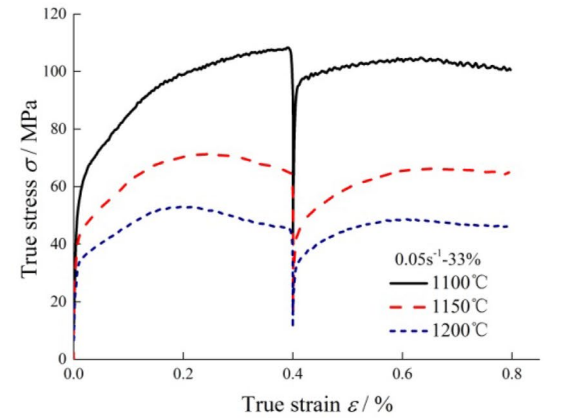

b Different temperatures under 0.05 s^{-1}-33%-5 s

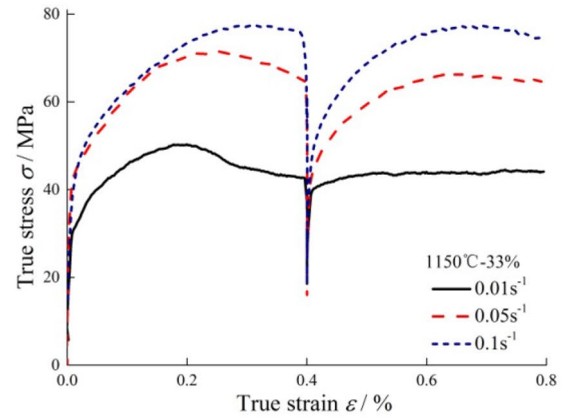

c Different strain rates under 1150 °C -33%-5 s

Figure 4 Typical true tress-strain curves under different deformation conditions and inter-pass times

resistance are large, and the flow stress increases as well. The flow stresses under different strain rates are shown in Figure 4(c), it is obviously that, the flow stresses increase with the increase of strain rate. This is due to the counteraction between work hardening and recrystallization softening during deformation. When under high strain rate, there has no enough time for the offset, and the increase of flow stress is the macroscopic performance of the increasing deformation resistance.

The calculation method for the MDRX softening fraction can be summarized [27–29] as:

$$X_{\mathrm{MDRX}} = \frac{\sigma_m - \sigma_2}{\sigma_m - \sigma_1}, \tag{1}$$

where X_{MDRX} is the MDRX softening fraction, σ_m is the flow stress at the interruption, σ_1 and σ_2 are the offset stress (0.2%) at the first and second deformation, respectively.

The kinetic models of MDRX are usually defined by the exponent-type equations [27–29] as follows:

$$X_{\mathrm{MDRX}} = 1 - \exp\left[-0.693\left(\frac{t}{t_{0.5}}\right)^{n_1}\right], \tag{2}$$

$$t_{0.5} = A_m \dot{\varepsilon}^{P_m} \exp\left(\frac{Q_{\mathrm{MDRX}}}{RT}\right), \tag{3}$$

where Q_{MDRX} is the apparent activation energy of MDRX, $t_{0.5}$ is the time for 50% MDRX, $\dot{\varepsilon}$ is the strain rate, T is the deformation temperature, R is the gas constant, A_m, P_m and n_1 are the material dependent constants. Taking natural logarithm on both sides of Eq. (2) and Eq. (3). Values of $t_{0.5}$ are illustrated in Table 3 and the other constants are easy to evaluate form Figure 5. The values of the constants are calculated as, $n_1 = 0.753$, $A_m = 1.33 \times 10^{18}$, $P_m = -0.41$ and $Q_{\mathrm{MDRX}} = 487.6$ kJ/mol, respectively.

The kinetic models of MDRX can be expressed as follows:

$$X_{\mathrm{MDRX}} = 1 - \exp\left[-0.693\left(\frac{t}{t_{0.5}}\right)^{0.753}\right], \tag{4}$$

$$t_{0.5} = 1.33 \times 10^{18} \dot{\varepsilon}^{-0.41} \exp\left(\frac{4876000}{RT}\right). \tag{5}$$

Comparisons of the calculated and experimental MDRX softening fraction X_{MDRX} at different

Table 3 Values of $t_{0.5}$ under different deformation conditions

Deformation conditions	$t_{0.5}$ (s)
1200 °C—0.05 s^{-1}—33%	1.09
1150 °C—0.01 s^{-1}—33%	5.01
1150 °C—0.05 s^{-1}—33%	3.25
1150 °C—0.1 s^{-1}—33%	1.83
1150 °C—0.05 s^{-1}—26%	5.23
1150 °C—0.05 s^{-1}—40%	1.58

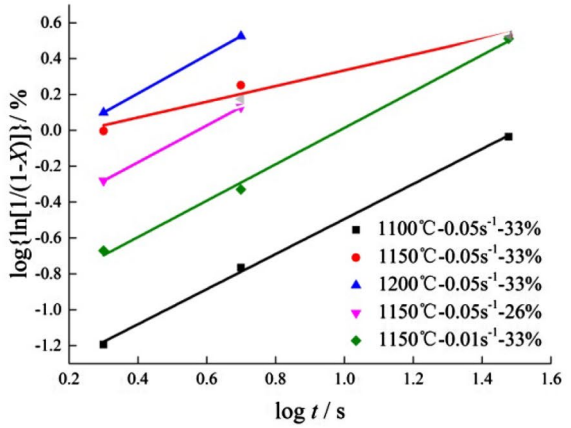

a Calculation on n_1

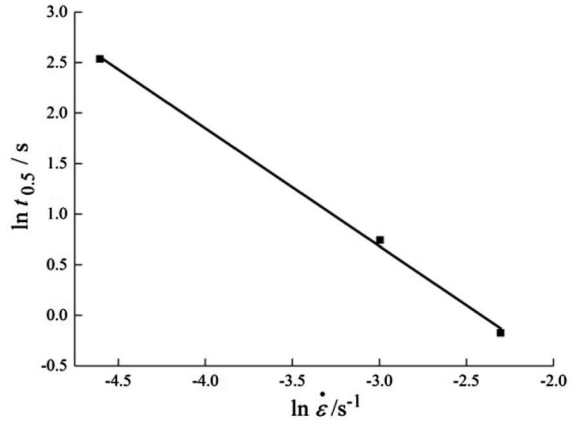

b Calculation on P_m

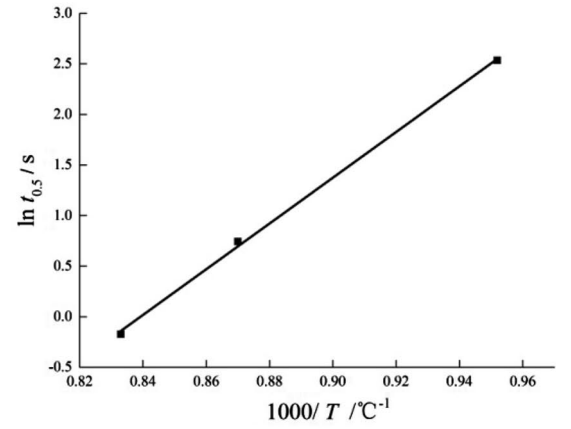

c Calculation on Q_{MDRX}

Figure 5 The calculations on the different constants of MDRX kinetic models

deformation conditions are illustrated in Figure 6. It can be shown that the predicted results are in good agreement with the experimental results, which confirms that the proposed models can give an accurate and precise estimate of MDRX behaviors for the studied as-cast P91 alloy steel.

3.2 MDRX Grain Size Model

The complete MDRX time $t_{0.95}$ is the time for 95% MDRX, and it can be calculated by Eqs. (4)–(5). After the first pass compression, the specimens were kept under deformation temperature at $t_{0.95}$ and directly quenched in water for holding the complete MDRX metallographic structures. Figure 7 illustrates the metallographic structures under different compression temperatures. The average MDRX grain sizes under different deformation conditions are shown in Table 4.

It can be found in Table 4, the average grain size of the complete MDRX increases with the increasing temperature and decreases with the increasing of strain rate or deformation degree. The grain size model of MDRX [27–29] is given below:

$$d_{\mathrm{MDRX}} = a_m d_0^{k_m} \dot{\varepsilon}^{h_m} \exp\left(\frac{-Q_{\mathrm{MDRX}}}{RT}\right), \tag{6}$$

where d_0 is the initial grain size, it can be obtained in Table 4 as well. The a_m, k_m and h_m are the materials dependent constants. Taking logarithm on both sides of Eq. (6), the constants k_m and h_m can be calculated through the linear fitting method. Figure 8(a) and (b)

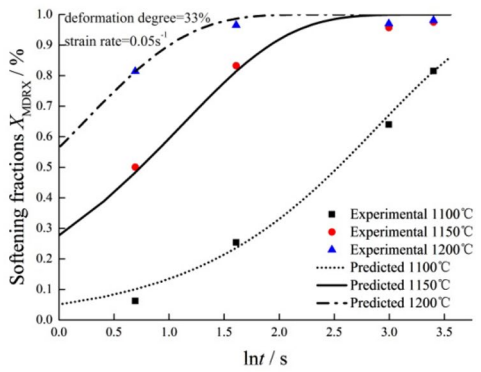

a Deformation degree of 33% and strain rate of 0.05 s^{-1}

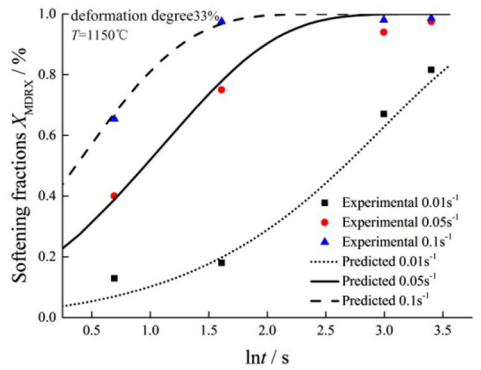

b Defomation degree of 33% and temperature of 1200 °C

Figure 6 Comparisons between the predicted and the experimental MDRX softening fraction under different deformation conditions

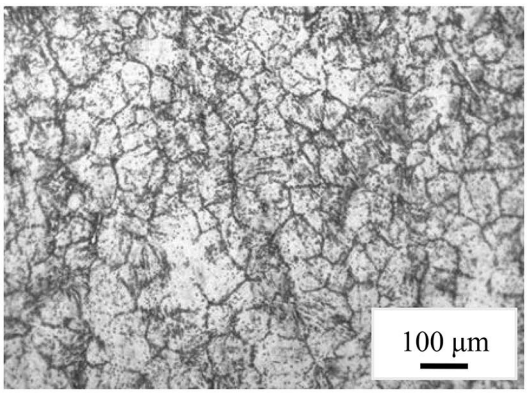

a 1200 °C

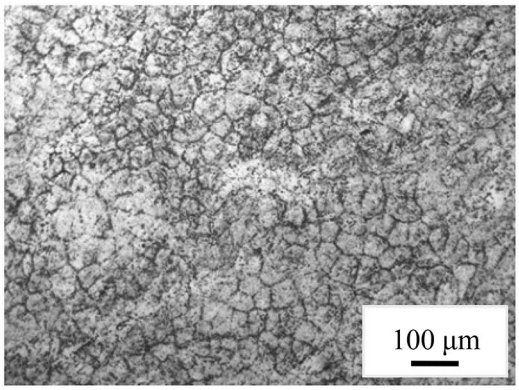

b 1150 °C

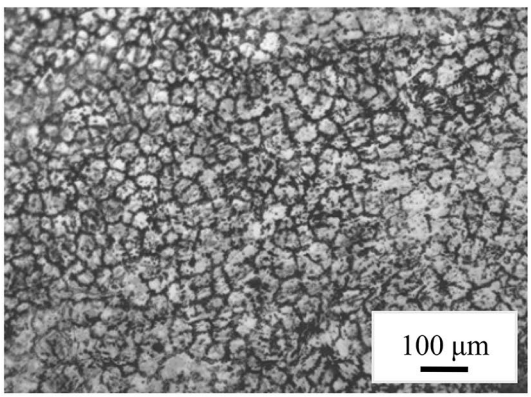

c 1100 °C

Figure 7 Complete MDRX metallographic structures under strain rate of 0.05 s^{-1} and deformation degree of 33%

shows the relationships between $\ln d_{MDRX}$-$\ln d_0$ and $\ln d_{MDRX}$-$\ln \dot{\varepsilon}$. By substituting the values of materials constants and forming parameters into Eq. (6), the value of a_m can be easily computed. The grain size model can be expressed as:

$$d_{MDRX} = 9.37 \times 10^{14} d_0^{2.03} \dot{\varepsilon}^{-0.2} \exp\left(\frac{-487598.64}{RT}\right). \quad (7)$$

Table 4 Average grain sizes of MDRX

Deformation conditions	d_0 (μm)	d_{MDRX} (μm)
1200 °C—0.05 s^{-1}—33%	123	27.4
1150 °C—0.01 s^{-1}—33%	103	23.2
1150 °C—0.05 s^{-1}—33%	103	20.9
1150 °C—0.1 s^{-1}—33%	103	14.7
1150 °C—0.05 s^{-1}—26%	103	24.6
1150 °C—0.05 s^{-1}—40%	103	19.1
1100 °C—0.05 s^{-1}—33%	89	14.1
1050 °C—0.05 s^{-1}—33%	80	12
1150 °C—0.5 s^{-1}—33%	103	11.3

In order to verify the MDRX grain size model of as-cast P91 alloy, comparisons between measured and predicted results were carried out in Figure 8(c). The correlation coefficient between the experimental and predicted results is 0.92. It can be found that the predicted results are in good agreement with the experimental ones, which indicated that the grain size model can give an accurate estimate of average MDRX grain size of hot deformed as-cast P91 alloy.

Therefore, the MDRX kinetic models and the grain size model can be applied to theoretical research of hot extrusion process.

4 Numerical Simulation

Hot extrusion FE model combined thermal-mechanical (constitutive model) with micro-macro (DRX models, MDRX models and grain growth model) of as-cast P91 alloy was further developed for simulation of the hot extrusion. Based on the hot extrusion FE model, the influences of hot extrusion parameters on the grain sizes of the extruded pipe were investigated and the optimum extrusion parameters were revealed.

4.1 Constitutive and Microstructural Models of As-cast P91 Alloy Steel

The flow stress constitutive models were expressed by Eqs. (8)–(10) from Ref. [25]. Moreover, Eqs. (11)–(15) are the DRX grain size model which obtained from Ref. [26]. The grain growth model is established in Eq. (16) form Ref. [25]. In these equations, Z is the Zener–Hollomon parameter which is a function of temperature and strain rate. ε_P is the peak strain, ε_c is the critical strain, X_{DRX} is the DRX volume fraction, $\varepsilon_{0.5}$ represents the strain of 50% DRX volume fraction and d_{DRX} is the average DRX grain size. d_G is the average grain growth size, t_1 is the growth time. Eqs. (17)–(19) are the above established MDRX models. All these models agree well with the experimental results.

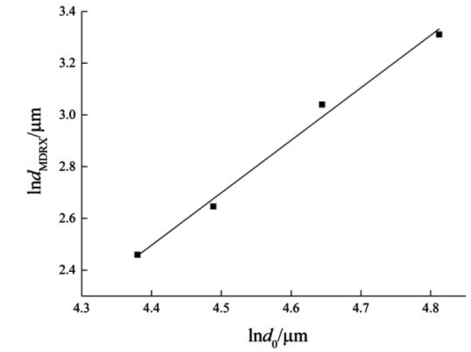

a Relationship between $\ln d_{\mathrm{MDRX}}$ and $\ln d_0$

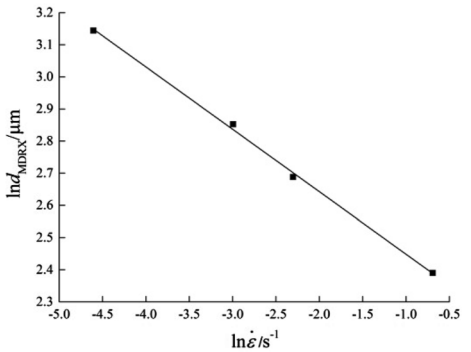

b Relationship between $\ln d_{\mathrm{MDRX}}$ and $\ln \dot{\varepsilon}$

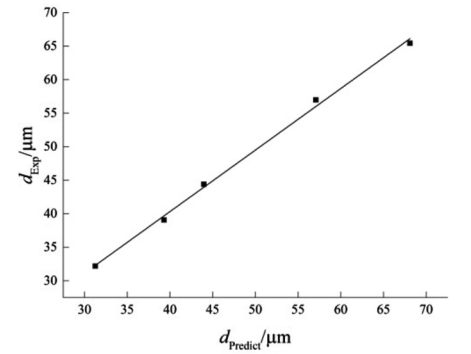

c Comparisons between the predict and the experimental data of complete MDRX grain sizes

Figure 8 Calculation on the different constants of MDRX grain size model and comparisons between the predict and the experimental data of complete MDRX grain sizes

$$\sigma = \frac{1}{0.008}\left\{\left(\frac{Z}{6.27\times10^{17}}\right)^{0.179} + \left[\left(\frac{Z}{6.27\times10^{17}}\right)^{0.357} + 1\right]^{0.5}\right\}, \tag{8}$$

$$\dot{\varepsilon} = 6.27\times10^{17}[\sinh(0.008\sigma)]^{5.6}\times\exp\left(-\frac{447719.1}{RT}\right), \tag{9}$$

$$Z = \dot{\varepsilon}\exp\left(\frac{447719.1}{RT}\right), \tag{10}$$

$$\varepsilon_P = 0.0162Z^{0.0863}, \tag{11}$$

$$\varepsilon_c = 0.867\varepsilon_P, \tag{12}$$

$$X_{\mathrm{DRX}} = 1-\exp\left[-1.125\left(\frac{\varepsilon-\varepsilon_c}{\varepsilon_{0.5}}\right)^{4.005}\right], \tag{13}$$

$$\varepsilon_{0.5} = 1.09\dot{\varepsilon}^{0.173}\exp\left(\frac{101601}{RT}\right), \tag{14}$$

$$d_{\mathrm{DRX}} = 3.65\times10^{4}Z^{-0.21}, \tag{15}$$

$$d_G^{2.68} = d_0^{2.68} + 1.58\times10^{8}t_1^{0.31}\exp\left(-\frac{79428}{RT}\right), \tag{16}$$

$$X_{\mathrm{MDRX}} = 1-\exp\left[-0.693\left(\frac{t}{t_{0.5}}\right)^{0.753}\right], \tag{17}$$

$$t_{0.5} = 1.33\times10^{18}\dot{\varepsilon}^{-0.41}\exp\left(\frac{4876000}{RT}\right), \tag{18}$$

$$d_{\mathrm{MDRX}} = 9.37\times10^{14}d_0^{2.03}\dot{\varepsilon}^{-0.2}\exp\left(\frac{-487598.64}{RT}\right). \tag{19}$$

4.2 Further Development of Hot Extrusion FE Model in DEFORM

The models of as-cast P91 alloy steel (Eqs. (8)–(19)) were encoded into subroutine code of DEFORM-3D platform by FORTRAN language. The microstructure evolution calculation procedures of the hot extrusion process are shown in Figure 9.

4.3 Hot Extrusion Geometrical Models and Numerical Simulation Parameters

Figure 10(a) shows the working principle of the vertical extrusion machine on heavy caliber thick-wall pipe. Considering the symmetric geometry of the billet, the die and the extrusion needle, 3D axisymmetric models are established in Figure 10(b). The required simulation conditions and parameters for the reliability simulation of hot extrusion FE model are shown in Table 5. The material of the die, the extrusion needle and the extrusion block were H-13 die steel (4Cr5MoSiV1). The glass lubricant was used in hot extrusion process and the friction coefficient was 0.04 [12].

4.4 Simulation Results and Analysis

In order to estimate the influences of different extrusion parameters on the grain size of extruded thick-wall pipe,

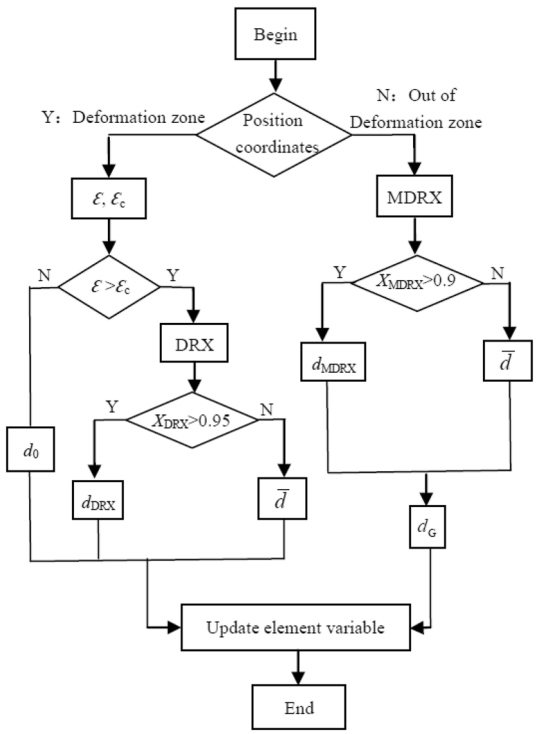

Figure 9 Microstructure evolution model of hot extrusion in subroutine code

the parameter K was proposed and defined by the functions in the following:

$$K = \frac{M}{N}, \tag{20}$$

$$N = \frac{P_{\max} - P_{\min}}{P_{\min}} \times 100\%, \tag{21}$$

$$M = \frac{d_{P\max} - d_{P\min}}{d_{P\min}} \times 100\%, \tag{22}$$

where N and M are the changing rates. $P_{\max}$, $P_{\min}$ are the maximum and minimum values of a specific parameter, while P is related to the temperature, the extrusion ratio and the extrusion speed, respectively. $d_{P\max}$, $d_{P\min}$ are the grain sizes under $P_{\max}$ and $P_{\min}$, respectively. When K is calculated as positive value, the grain size increases with the increasing parameter, on the contrary, the value of K is negative and the grain will refined with the increase of parameter value.

Figure 11 shows the grain size distribution of the simulated pipe during hot extrusion. Part A is the top of the pipe and part B is the end of the pipe. The grain sizes of part A are larger than other part because of the

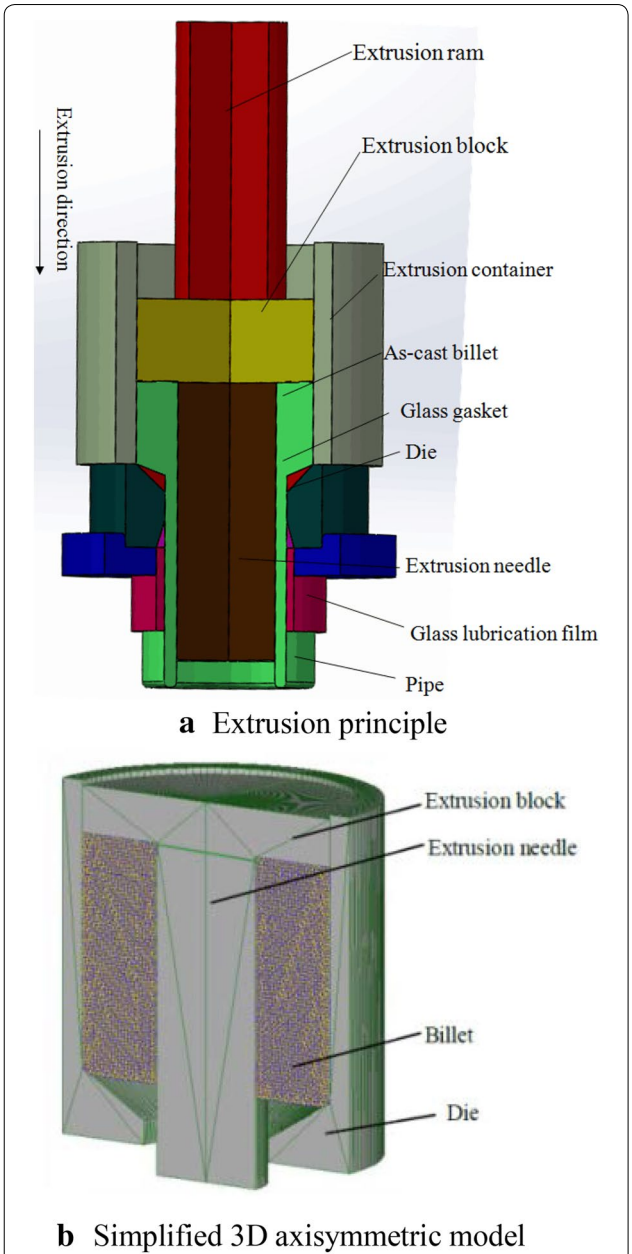

Figure 10 The extrusion working principle and 3D model

inhomogeneous deformation of the billet, and it is usually removed in the industrial production. After hot extrusion, the microstructures of the end part are the finest and smallest in the pipe, while the length of this part is relatively short. Hence, the proper observation area of the pipe is the middle part shown in Figure 12 (pipe extruded in stable stage). The inner and outer surface will be finish cut in the future process, so points 1 and 5 are about 5 mm from the surface and the five points are equidistributed in the cross section. The

Table 5 Hot extrusion parameters for the coupled hot extrusion FE model

Parameter	Content
Pipe size (mm)	φ630 × φ500 × 9000
Initial billet temperature (°C)	1150, 1200, 1250
Initial die temperature (°C)	300
Initial grain size (μm)	123
Extrusion ratio	5, 7, 9
Extrusion speed (mm/s)	30, 40, 50
Die taper angle (°)	42
Coulomb friction coefficient	0.04
Thermal emissivity of blank	0.7
Environment temperature (°C)	20
Heat convection coefficient between billet and extrusion tools (N/mm/s/°C)	11
Heat convection coefficient between billet and air (N/mm/s/°C)	0.02

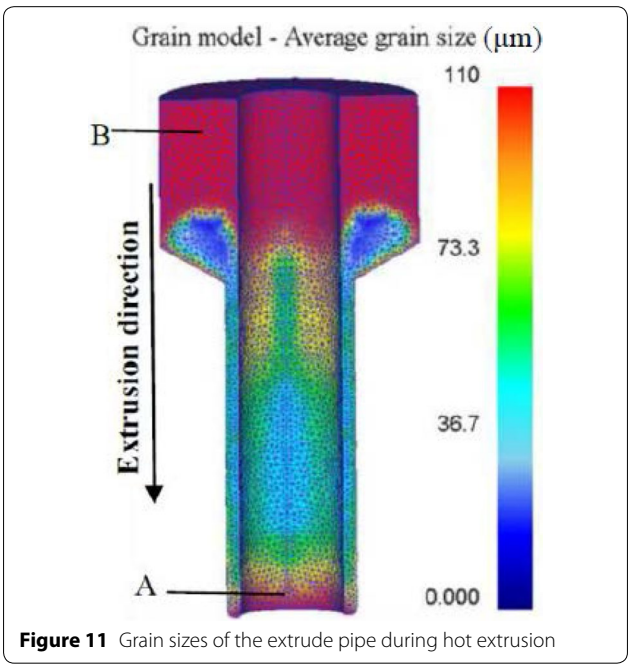

Figure 11 Grain sizes of the extrude pipe during hot extrusion

effects of extrusion parameters on average grain size are analyzed in below.

4.4.1 Initial Extrusion Temperature

Figure 13(a) shows the effect of the initial extrusion temperature on the grain sizes and the DRX volume fractions of the pipe in extrusion stable stage, the extrusion ratio was 9 and the extrusion speed was 40 mm/s.

It is found that the DRX volume fractions of the five observation points are increasing as the temperature

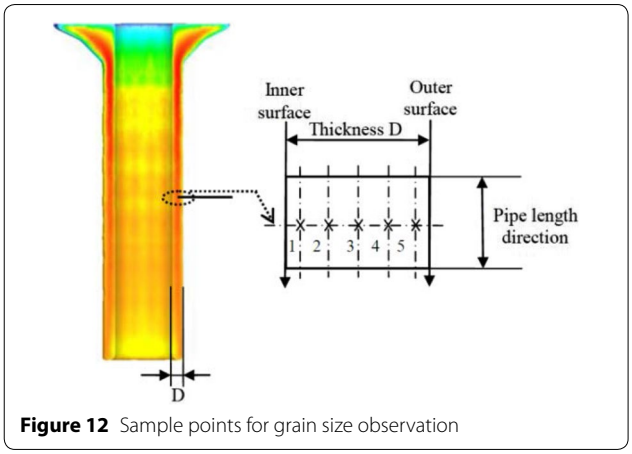

Figure 12 Sample points for grain size observation

increases. High deformation temperature offers enough energy for the nucleation and grain growth of DRX, and the atoms diffusion, grain boundary migrations are enhanced as well. Such phenomenon may owe to the fact that, during hot deformation, the boundary migration speed of the ridged-shape grains are fast and the migrations will grow into new recrystallization grains in a short time. In addition, due to the migrations and continuous deformation, the dislocation density behind the grain boundary is sharply decreased, which could not achieve to the balance state in a short time. Thus the decreasing dislocation density provides advantages for the nucleation of new grains. When the deformation temperature is low (in Figure 13(a) of 1150 °C), the grain boundary migration does not have enough driving force, the growth of the potential crystal nucleus will stop and even disappear due to the surface energy. So under lower deformation temperature, the DRX volume fraction is smaller. The DRX volume fractions under 1250 °C are more uniform and the values can achieve to more than 95%.

The average grain size increases as temperature increase which is due to the exponential increase on grain growth under high temperature. Furthermore, the optimum extrusion temperature is 1250 °C, the parameter K of initial extrusion temperature on average grain size is calculated as 3.17.

4.4.2 Extrusion Speed

The effect of the extrusion speed on the average grain sizes and DRX volume fractions of the pipe in extrusion stable stage can be found in Figure 13(b), when the extrusion temperature was 1200 °C and the extrusion ratio was 9.

The average grain size and DRX volume fraction increase with the increasing extrusion speed. As simulated in the hot extrusion process, the peak values of the strain rate under different extrusion speed (30 mm/s,

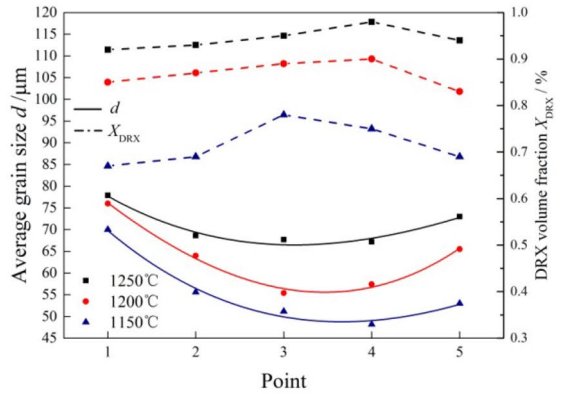

a Initial extrusion temperature

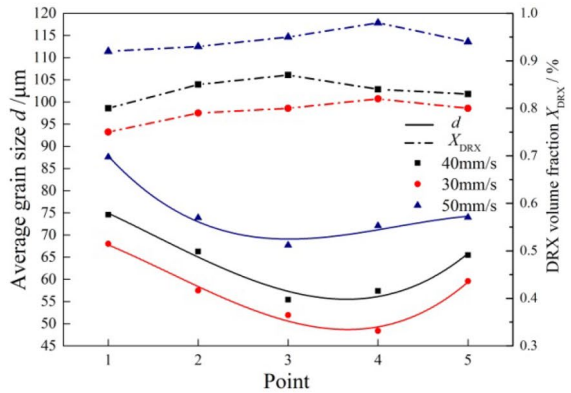

b Extrusion speed

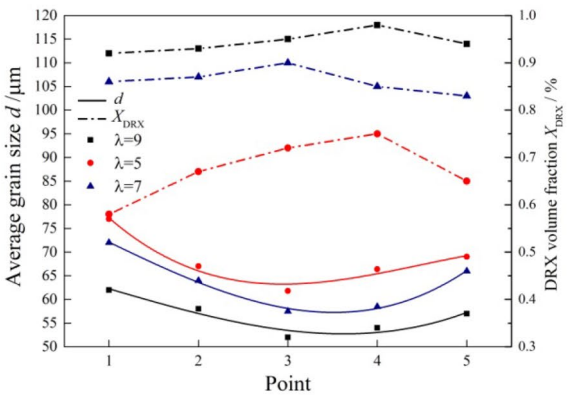

c Extrusion ratio

Figure 13 Effects of extrusion parameters on grain sizes and DRX volume fractions in stable stage

40 mm/s and 50 mm/s) were 16.6 s^{-1}, 19.6 s^{-1} and 24.3 s^{-1}, respectively. It can be found in hot compression tests [24], the grain size decreases with the increase of strain rate and the DRX volume fraction increases with the increasing strain rate. However, in Figure 13(b), the grain size changes in a totally opposite rule of the compression experiments. This phenomenon can be explained by the increased temperature. During the extrusion process, the deformation spaces consist of the billet, the extrusion die and the extrusion needle. The spaces are nearly under an adiabatic condition, the heat transfer only occurs between the three parts, and higher extrusion speed brings large friction heat. The maximum temperatures during hot extrusion under extrusion speed of 30 mm/s, 40 mm/s and 50 mm/s were 1230 °C, 1250 °C and 1290 °C, respectively. When the extrusion speed is higher, the time of DRX nucleation and growth is getting shorter. Even though there have generated more heat which offer to the recrystallization nucleation, but the nucleation grains do not have adequate time to complete the grain boundary migration and dislocation energy accumulation. Thus, the increased fiction heat is used to the grain growth instead. So the grain size increases with the increase of extrusion speed, besides the microstructural evolution of as-cast P91 alloy steel is more sensitive to the temperature than the strain rate.

For this reason, if the initial extrusion temperature is high, the extrusion speed should not fast. The parameter K of extrusion speed on average grain size is calculated as 0.41, and the optimum extrusion speed is 50 mm/s.

4.4.3 Extrusion Ratio

In the industrial production, the extrusion ratios are determined by the billet size and die mold. The effect of extrusion ratio on the average grain sizes and DRX volume fractions of the pipe in extrusion stable stage is presented in Figure 13(c), when the extrusion temperature was 1200 °C and the extrusion speed was 40 mm/s.

It can be obtained that, larger extrusion ratio induces higher DRX volume fractions and finer grain sizes because of the increased deformation degree. Under large extrusion ratio, the nucleation positions of the recrystallization grains and the driving force for the grain growth are increased during deformation. Thus the DRX volume fractions under extrusion ratios of 9 are nearly 100%, so the optimum extrusion ratio is 9.

The parameter K of extrusion ratio on average grain size is calculated as -0.814. Under the capacity of the extrusion machine, it is better to use the large extrusion ratio and the slow extrusion speed.

4.4.4 Effects of Key Extrusion Parameters on Grain Size

As discussed above, the extrusion parameters of initial temperature, extrusion speed and extrusion ratio are mainly influence the grain sizes of the extruded pipe. Initial temperature and extrusion speed have positive influence on the grain sizes, while the extrusion ratio has negative influence. In contrast, the grain size is more sensitive to the temperature, and the extrusion ratio and speed have less effect on it. Thus, the design and optimization on CHE hot extrusion parameters must firstly determine the initial extrusion temperature, and then the

extrusion ratio. Under the invariability extrusion ratio, to obtain the heavy caliber thick-wall pipes with finer and smaller grains, the extrusion speed should not fast.

In the extrusion stable stage, the average grain sizes of the whole pipe are inhomogeneous. In the length direction, part A are the biggest and part B are the smallest, in the cross section, the middle part are smaller than the two sides. The main reason is the nonuniform deformations during the extrusion. In the length direction, the billet is under the constraint pressure and external friction from the die, the outer surface is under the additional shear deformation, therefore the materials flow out of the extrusion die in a nonuniform speed. Similarly, in the cross section of the pipe, the materials in outer and inner surface are under the shear deformation. Although the extrusion ram moves in a uniform velocity, but the flow speed of the materials during extrusion is nonuniform. In addition, another nonuniform factor is the temperature gradient of the billet during hot extrusion, and it is higher in the middle and lower in the two sides due to the heat exchanges with die and extrusion needle.

To summarize, the optimum hot extrusion parameters of CHE process are including that, the initial temperature of 1250 °C, the extrusion ratio of 9 and extrusion speed of 50 mm/s.

5 Hot Extrusion Experiment on Heavy Caliber Thick-Wall Pipe

The hot extrusion experiment was carried out under the conditions of the proposed extrusion parameters in Hebei Hongrun Nuclear Equipment Technology Industry Co., Ltd. The 500 MN vertical hot extrusion equipment (Figure 14(a)) was employed to investigate the hot extrusion process. The P91 as-cast billet and the extruded pipe are shown in Figure 14(b) and (c), respectively. The initial temperature of the billet was 1250 °C, the initial temperature of the die and extrusion needle were 300 °C, and the taper angle of the extrusion die was 42°. The billet size was ϕ1253 mm × ϕ500 mm × 1000 mm and the production pipe size was ϕ630 mm × ϕ500 mm × 8500 mm. The glass lubrication gasket with 80 mm in height was placed between the billet and the extrusion block. The load–displacement curve of the extrusion ram was recorded during the extrusion process. The specimens (Figure 12) were cut from the middle part of the pipe which shown in Figure 14(d).

The comparisons between the measured and simulated load–displacement curves are illustrated in Figure 15. The results show that, the maximum load value of the experiment is 430 MN, while the simulation load is 415 MN. The difference mainly due to the simplification of the hot extrusion FE model, and the actual extrusion fraction conditions are more complicated than the simulated. Thus the difference of the load value is in a reasonable deviation range. The computed results present a good estimate of the relationship between load and displacement during the hot extrusion process.

The metallographic structures of the five points are shown in Figure 16, the grain sizes are measured and compared with the simulated results as well. It can be found that the averaged grain sizes of the extruded pipe are about 60 μm, and the structures are fine and uniform. The experimental results are larger than the simulation ones due to the high temperature of the production environment. Whatever, the measured results and simulated data has good agreement, and the largest mean error is

a The 500 MN vertical hot extrusion equipment **b** As-cast P91 billet **c** Extruded pipe **d** Experiment sample

Figure 14 Hot extrusion experiment on heavy caliber thick-wall pipe

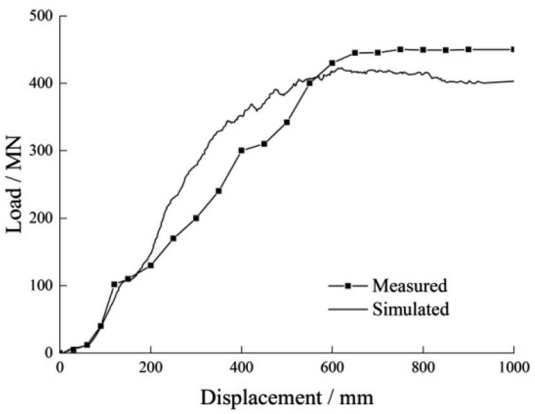

Figure 15 Comparisons of displacement—load curves between measured and simulated

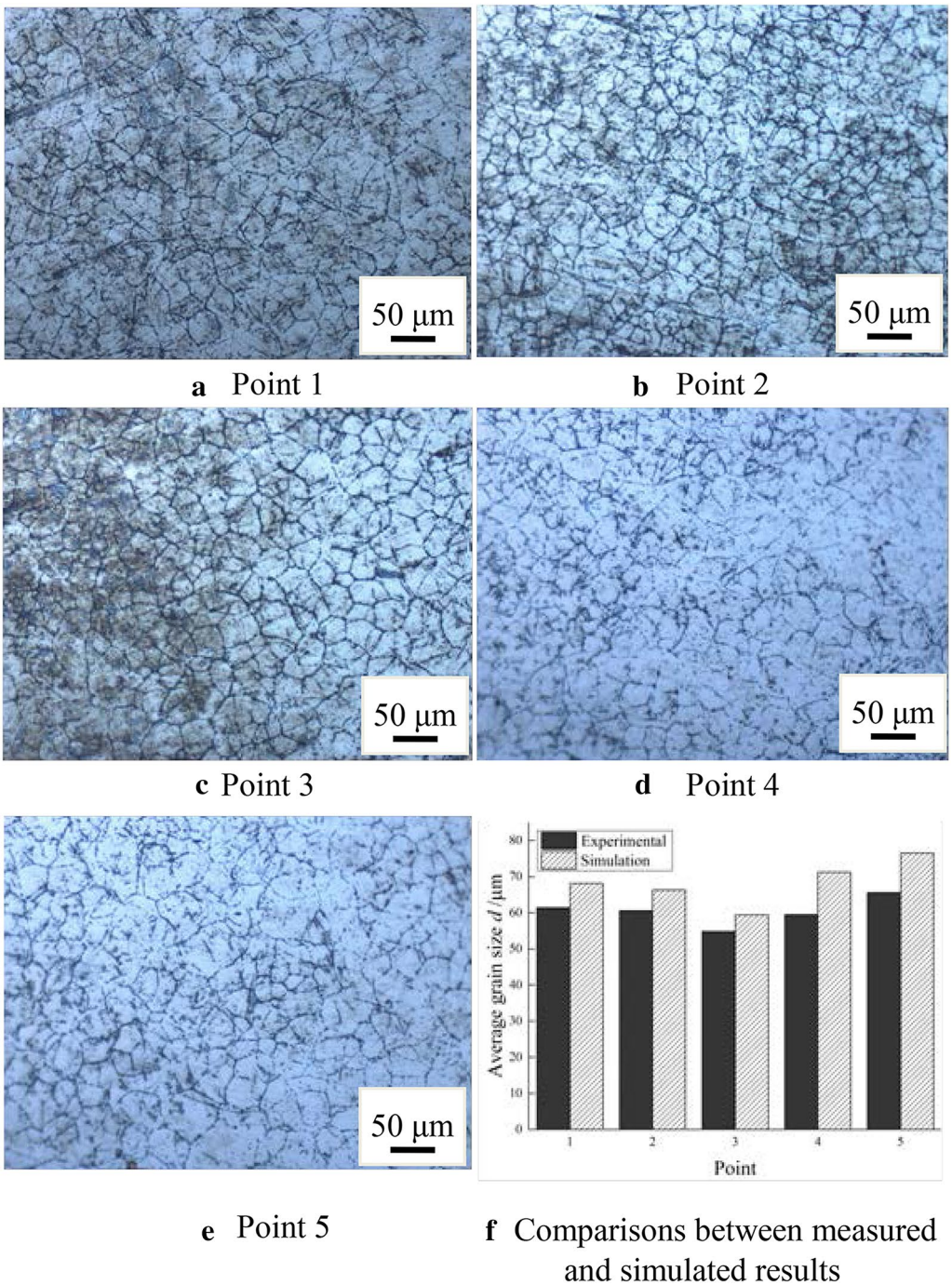

Figure 16 The metallographic structures of extruded pipe and the grain sizes comparisons between measured and simulated results

20% which appears in point 4. Thus the proposed constitutive equations and microstructural evolution models present a good estimate of hot deformation behaviors of as-cast P91 alloy. Meanwhile, the hot extrusion FE model can be used in the simulation analysis, it offers guidance for the industrial production research of CHE process.

6 Conclusions

(1) According to the hot compression tests, the MDRX behaviors of as-cast P91 alloy are investigated. The MDRX kinetic models and grain size model are

proposed, which are consistent with the related experimental results.

(2) The thermal-mechanical and micro-macro coupled hot extrusion FE model are established to predict the microstructural evolution behaviours during hot extrusion of as-cast P91 alloy. The hot extrusion FE models are encoded into the DEFORM-3D platform by FORTRAN language.

(3) Effects of extrusion parameters on grain sizes of the extruded pipe are investigated by FE simulations. The grain size increases with the increase of initial temperature and extrusion speed, and it decreases with the increase of extrusion ratio. In contrast, the grain size is most sensitive to the temperature and then the extrusion ratio. In order to obtain the fine and uniform grain microstructures, the optimum hot extrusion parameters are including that, initial temperature of 1250 °C, the extrusion ratio of 9 and extrusion speed of 50 mm/s.

(4) The hot extrusion verification experiment is performed on 500 MN vertical hot extrusion equipment under the proposed extrusion parameters. The load-displacement curve during the extrusion experiment and the grain sizes of the middle part extruded pipe present good consistent with the simulation results. The coupled hot extrusion FE model could give a good estimate of hot extrusion behaviors of as-cast P91 alloy. It can be used to guide the industrial production research of CHE process.

Authors' Contributions

YL was in charge of the whole trial; LJ wrote the manuscript; LJ, TH and YZ assisted with sampling and laboratory analyses. All authors read and approved the final manuscript.

Author Details

[1] Department of Mechanical Engineering, Taiyuan Institute of Technology, Taiyuan 030008, China. [2] Shanxi Key Laboratory of Metallic Materials Forming Theory and Technology, Taiyuan University of Science and Technology, Taiyuan 030024, China. [3] School of Materials Science and Engineering, Taiyuan University of Science and Technology, Taiyuan 030024, China. [4] Hebei Hongrun Nuclear Equipment Technology Industry Co., Ltd, Cangzhou 061300, China.

Authors' Information

Lu Jia, born in 1989, is currently a lecturer at *Taiyuan Institute of Technology, China*. She received her PhD degree from *Taiyuan University of Science and Technology, China*, in 2017. Her research interests including advanced manufacturing technology and numeral simulating & emulating.

Yongtang Li, born in 1957, is currently a professor at *Taiyuan University of Science and Technology, China*. He received his PhD degree from *Tsinghua University, China*, in 1994. His research interests include advanced manufacturing technology, forging equipment and theory and compact production process.

Tianjing Hui, born in 1991, is currently a master candidate at *Taiyuan University of Science and Technology, China*.

Yang Zhang, born in 1989, is currently an assistant engineer at *Hebei Hongrun Nuclear Equipment Technology Industry Co., Ltd, China*

Competing Interests

The authors declare that they have no competing interests.

Funding

Supported by National Natural Science Foundation of China (Grant Nos. 51675361, 51135007), Shanxi Scholarship Council of China (Grant Nos. 2015-086, 2016-096), and Shanxi Provincial Key Research and Development Program of China (Grant No. 03012015004).

Publisher's Note

Received: 29 March 2017 Accepted: 8 January 2019
Published online: 30 January 2019

References

[1] Y Li, W Q Huang, X H Chang, et al. A practical and selective method for the analysis of molybdenum in grad T91 tube and P91 pipe intended for power plants. *Materials and Design*, 2011, 284–286: 1510–1515.

[2] Y R Guo, H Wu. Progress of research on production localization of P91 seamLess steel tube. *Steel Pipe*, 2008, 37(1): 22–27. (in Chinese)

[3] R J Wang, Y G Xu, W Chen, et al. The property and application of P91 resistant steel for ultra- supercritical boilers. *Modern Metallurgy*, 2009, 37(3): 1–3. (in Chinese)

[4] Y T Li, L Jia, J H Fu. Thick-walled seamLess steel tube short tube short process casting and squeezing continuous formation method: China, ZL201310025737.4. [2015-08-19]. http://www.pss-system.gov.cn/sipopublicsearch/patentsearch/showViewList-jumpToView.shtml.

[5] F C Qin, Y T Li, H P Qi, et al. Method for producing heavy-caliber thick-walled seamLess steel pipe by casting extrusion composite molding: China, CN201510172364.2. [2015-04-13]. http://www.pss-system.gov.cn/sipopublicsearch/patentsearch/showViewList-jumpToView.shtml.

[6] G H Chelu, N Ghian. Technological parameters influence on the hot extrusion force of the pipes. *Chemistry and Materials Science*, 2002, 64(4): 47–56.

[7] C Y Sun, B Liu, R Li, et al. The temperature rise and extrusion force of IN690 superalloy during tube hot extrusion process. *Material Science and Technology*, 2011, 19(4): 52–58.

[8] J Chen, C G Bao, F L Chen. Evolutions of microstructure and mechanical properties for Mg-Al/AlN composites under hot extrusion. *Materials Science and Engineering A*, 2016, 667: 426–434.

[9] L Dang, H Yang, L G Huo, et al. DRX rules during extrusion process of large-scale thick-walled Inconel 625 pipe by FE method. *Transactions of Nonferrous Metals Society of China*, 2015, 25: 3037–3047.

[10] L L Chang, Y N Wang, X Zhao. Modeling of severe deformation and mechanical properties in Mg-3Al-1Zn alloy through asymmetric hot-extrusion. *Transactions of Nonferrous Metals Society of China,* 2008, 18: 257–262.

[11] H Jiang, J X Dong, M C Zhang, et al. Phenomenological model for the effect of strain rate on recrystallization and grain growth kinetics in the 617B alloy. *Journal of Alloys and Compounds*, 2018, 735: 1520–1535.

[12] D Sathishkumar, P Sivakumar K S Sundaram, et al. Finite element analysis and experimental study on the effect of extrusion ratio during hot extrusion process of aluminium matrix composites. *Defence Science Journal*, 2017, 67(4): 428–436.

[13] T Tang, Y C Shao, D Y Li, et al. Extrusion simulation and texture study on Mg-Y alloy. *Materials Science Forum*, 2014, 817: 531–537.

[14] Sasaki, Terufumi, Kobayashi, et al. Production and properties of seamless modified 9Cr-1Mo steel boiler pipes. *Kawasaki Steel Technical Report*, 1991, 25: 78–87.

[15] C Pandey, A Giri, M M Mahapatra. Evolution of phases in P91 steel in various heat treatment conditions and their effect on microstructure stability and mechanical properties. *Materials Science and Engineering: A*, 2016, 664: 58–74.

[16] Y Q Cai, J Z Sun, C J Liu, et al. Relationship between dislocation density in P91 steel and its nonlinear ultrasonic parameter. *Journal of Iron and Steel Research, International*, 2015, 22(11): 1024–1030.

[17] M F Moreno. Application of small punch testing on the mechanical and microstructural characterizations of P91 steel at room temperature. *International Journal of Pressure Vessels and Piping*, 2016, 142–143: 1–9.
[18] L Jia, Y T Li, Y Zhang. A characterization for the deformation behavior of as-cast P91 alloy steel and utilization in hot extrusion process. *Advances in Materials Science and Engineering*, 2017, 2017: 1–11.
[19] M H Maghsoudi, A Z Hanzaki, P Changizian, et al. Metadynamic recrystallization behavior of AZ 61 magnesium alloy. *Materials and Design*, 2014, 57: 478–493.
[20] Y C Lin, L T Li, Y C Xia. A new method to predict the metadynamic recrystallization behavior in 2124 aluminum alloy. *Computational Materials Science*, 2011, 50: 2038–2043.
[21] Y C Lin, M S Chen, J Zhong. Study of metadynamic recrystallization behaviors in a low alloy steel. *Journal of Materials Processing Technology*, 2009, 209: 2477–2482.
[22] Y C Lin, M S Chen. Study of microstructural evolution during metadynamic recrystallization in a low-alloy steel. *Materials Science and Engineering A*, 2009, 501: 229–234.
[23] H Beladi, P Cizek, P D Hodgson. The mechanism of metadynamic softening in austenite after complete dynamic recrystallization. *Scripta Materialia*, 2010, 62: 191–194.
[24] Z X Li. *The microstructure analysis and numerical simulation for hot extrusion forming based on thick-wall pipe of as-cast P91 steel*. Taiyuan: Taiyuan University of Science and Technology, 2016. (in Chinese)
[25] K Deng. *Investigation of hot deformation behavior and structure property of as-cast P91 alloy based on thick walled pipe casting-extrusion composite forming*. Taiyuan: Taiyuan University of Science and Technology, 2015. (in Chinese)
[26] Z X Li, B F Lei, J H Fu, et al. Modeling of dynamic recrystallization for as-cast heat-resistant alloy steel P91. *Forging & Stamping Technology*, 2016, 41(1): 121–126. (in Chinese)
[27] A Paggi, G Angella, R Donnini. Strain induced grain boundary migration effects on grain growth of an austenitic stainless steel during static and metadynamic recrystallization. *Materials Characterization*, 2015, 107: 174–181.
[28] P Uranga, A I Ferbabdez, B Lopez, et al. Transition between static and metadynamic recrystallization kinetics in coarse Nb microalloyed austenite. *Materials Science and Engineering A*, 2003, 345: 319–327.
[29] S Cho, K Kang, J Jonas. The dynamic, static and metadynamic recrystallization of a Nb-microalloyed steel. *ISIJ International*, 2001, 41(1): 63–69.